Improved Basis Sets in the Linearized Augmented Planewaves plus Local Orbitals Method

Bachelor's Thesis

for obtaining the degree
Bachelor of Science (B. Sc.)

Humboldt-Universtät zu Berlin
Faculty of Mathematics and Natural Sciences
Department of Physics

Author:	Hannah Kleine
Email:	hannah.kleine@physik.hu-berlin.de
Primary examiner:	Prof. Dr. Claudia Draxl
Secondary examiner:	Dr. Pasquale Pavone
Date of submission:	November 17th, 2021

Contents

1. Introduction

The development of many technologies requires investigation of novel, advanced materials with exceptional properties. Prominent examples are more efficient solar cells that can be used to solve one of today's most crucial problems — the global energy supply without fossil fuels. To this extent, a vast range of materials needs to be investigated. To do that efficiently, numerical modeling is a valuable addition to laboratory experiments. High-throughput calculations for example allow for investigations of a wide range of materials in short periods of time and therefore can speed up the discovery of new materials with outstanding properties.

With the ongoing advance of computer power, a broad range of different numerical methods have been developed. A widely used approach is Kohn-Sham density-functional theory (DFT). This *ab initio* method is able to provide ground-state properties for a broad spectrum of different materials ranging from bulk crystals to nanostructures. Over the years, a variety of different DFT implementations have been published. These implementations differ, among other things, in the choice of basis sets.

This work is concentrated on the all-electron full-potential computer package `exciting` [1]. We focus in particular on the implemented basis set, being the linearized augmented planewaves and local orbitals method ((L)APW+LO) and show how it can be improved. Thereby, we look at two different aspects.

On the one hand, we discuss how the generation of required input can be simplified and become more independent of the computed material. Thus, not only the usability of the code is simplified, it also improves the reproducibility and prepares it for possible high-throughput calculations. On the other hand, we discuss a more specific improvement of the description of a physical property — the spin-orbit coupling (SOC). It is especially important for materials containing heavier elements such as lead. In the development of solar-cells, hybrid organic/inorganic perovskites $CH_3NH_3PbX_3$ (X = Br, I) were found to be a promising choice of material. Because of the presence of lead, SOC effects play an important role in the computation of the electronic band structure. Without accounting for SOC-splitting e.g., the band gaps are strongly overestimated [2]. In order to capture such materials as well, we discuss how the treatment of SOC in the LAPW+LO framework can be improved.

2. Theoretical Background

2.1. Density-Functional Theory

The idea of representing a quantum system by its density existed many years before density-functional theory was formally developed. It was only in 1964 that Hohenberg and Kohn were able to show that the total energy $E_{\text{tot}}[n]$ of an interacting electron system in an external potential can be defined only by a functional of the ground-state electron density n, since there is a one-to-one correspondence between the potential and the density. In addition to that, they were able to show that the total energy obeys a variational principal with respect to the ground-state density [3].

Although this theorem formed the basis of DFT, it provides no instructions on how to actually perform calculations. A solution for this problem was proposed only one year later. Kohn and Sham stated that one could model the interacting many-body system by a non-interacting system with the same electron density as the original one [4]. Since the problem is now reduced to an effective single particle problem, it can be represented by the Kohn-Sham (KS) equations

$$\left[-\frac{1}{2}\nabla^2 + v_{\text{KS}}(\boldsymbol{r}) \right] \psi_{i\boldsymbol{k}}(\boldsymbol{r}) = \epsilon_{i\boldsymbol{k}} \psi_{i\boldsymbol{k}}(\boldsymbol{r}), \tag{2.1}$$

where $\boldsymbol{k}$ represents the wave vectors and $\boldsymbol{r}$ the space coordinates. $\epsilon_{i\boldsymbol{k}}$ are the eigenvalues, $v_{\text{KS}}(\boldsymbol{r})$ is the effective potential of the Kohn-Sham system, and $\psi_{i\boldsymbol{k}}(\boldsymbol{r})$ are the wavefunctions. The effective potential contains the Hartree potential v_{H}, the external potential v_{ext} given by the nuclei, and the unknown exchange-correlation potential v_{xc}, where both v_{H} and v_{xc} depend on the electron density n

$$v_{\text{KS}}(\boldsymbol{r}) = v_{\text{ext}} + v_{\text{H}}[n] + v_{\text{xc}}[n] \tag{2.2}$$

The density can be written in terms of the Kohn-Sham orbitals

$$n(\boldsymbol{r}) = \sum_{\boldsymbol{k}} w_{\boldsymbol{k}} \sum_{i} f_{i\boldsymbol{k}} |\psi_{i\boldsymbol{k}}(\boldsymbol{r})|^2, \tag{2.3}$$

where $w_{\boldsymbol{k}}$ is the weight of the $\boldsymbol{k}$-point and $f_{i\boldsymbol{k}}$ represents the occupation number. The Kohn-Sham equations are exact in theory and give the exact ground-state density. Nevertheless, it is not possible to get the exact solution, since the exchange-correlation (xc) potential is unknown and needs to be approximated. Over the years, several approximations have been developed. The most simple one is the local-density approximation (LDA), where the xc potential is locally replaced by the one of a homogeneous electron gas with the same electron density as that of the actual system [5]. This approximation leads to reasonable results for the total energies of metals, but for example strongly underestimates bond lengths.

Starting from LDA the generalized gradient approximation (GGA) has been developed by considering not only the local density but also the density gradient [6]. This results in improved total energies and more accurate lattice parameters, but e.g. band gaps are still underestimated. A way to compute band gaps more accurately, is to include a portion of exact Hartree-Fock exchange into the functional. These hybrid functionals give reasonable results for band gaps, but are computational expensive [7]. The choice of the appropriate functional depends on the material as well as the property of interest.

If one has chosen a functional, the Kohn-Sham equations need to be solved. There are two main approaches for doing so. One can either solve them numerically on a grid, or use a set of basis functions to form the the Kohn-Sham orbitals. The latter approach is the most common one and there are various different methods for constructing the basis which differ in efficiency and accuracy. The general expression for the expansion of the Kohn-Sham orbitals $\psi_{i\boldsymbol{k}}(\boldsymbol{r})$ in terms of basis functions $\phi_j(\boldsymbol{r})$ is the following:

$$\psi_{i\boldsymbol{k}}(\boldsymbol{r}) = \sum_j C_{ij}^{\boldsymbol{k}} \phi_j(\boldsymbol{r}). \tag{2.4}$$

One of the difficulties of modeling wavefunctions is their diverse behavior in space. Wavefunctions vary strongly near the nuclei while they vary slowly in between atoms. One method for treating this difficulty is to use pseudopotentials in the core regions. These potentials lead to smooth pseudo-wavefunctions and therefore, one can use a finite planewave basis to model the wavefunctions. Planewave basis sets are known to be quite efficient and relatively easy to implement, but they have some drawbacks as well. The complexity of the problem does not just vanish, but is transferred to the construction of the pseudopotentials. Additionally, the treatment of core states is strongly simplified and therefore not always reliable.

A way to avoid pseudopotentials is to divide the space into spherical muffin-tin (MT) and interstitial regions. Wavefunctions are treated differently in these areas. In this work, we concentrate on the latter method and to be more precise on the (linearized) augmented planewave plus local orbitals ((L)APW+LO) basis set implemented in `exciting`.

2.2. Augmented Planewaves

Firstly, we take a look at augmented planewaves (APW). The APW method was first developed in 1937 by Slater [8]. He proposed the use of planewaves in the interstitial regions as the they solve the Schrödinger equation (SE) in a constant potential. The potential in the MT spheres, which are centered around atoms α, can roughly be approximated by a spherical potential. Therefore, the basis functions in the MT are given by the solution to the SE in such spherical potential. The resulting basis functions take the following form

$$\phi_{\boldsymbol{G}+\boldsymbol{k}}(\boldsymbol{r}) = \begin{cases} \sum_{lm} A_{lm\alpha}^{\boldsymbol{G}+\boldsymbol{k}} u_{l\alpha}(r_\alpha) Y_{lm}(\hat{\boldsymbol{r}}_\alpha), & r_\alpha \leq R_{MT} \\ \frac{1}{\sqrt{\Omega}} e^{i(\boldsymbol{G}+\boldsymbol{k})\boldsymbol{r}}, & \boldsymbol{r} \in I. \end{cases} \tag{2.5}$$

Here, $\boldsymbol{G}$ represents the reciprocal lattice vectors, l stands for the azimuthal quantum number, m for the magnetic quantum number, $A_{lm\alpha}^{\boldsymbol{G}+\boldsymbol{k}}$ are expansion coefficients used to make $\phi_{\boldsymbol{G}+\boldsymbol{k}}(\boldsymbol{r})$

continuous at the boundary of the muffin-tin spheres, Ω is the unit cell volume, $Y_{lm}(\hat{\boldsymbol{r}}_\alpha)$ are the spherical harmonics, and $u_{l\alpha}(r_\alpha)$ the solutions of the radial Schrödinger equation

$$\left[-\frac{1}{2}\frac{d^2}{dr^2} + \frac{l(l+1)}{2r^2} + v_0(r) - \epsilon_{i\boldsymbol{k}} \right] r u_{l\alpha}(r) = 0, \tag{2.6}$$

where the parameters $\epsilon_{i\boldsymbol{k}}$ represent the eigenenergies of the KS-equation (2.1) and $v_0(r)$ is the spherical average of the KS-potential $v_{\mathrm{KS}}(\boldsymbol{r})$. When the radial SE is used, no relativistic effects are considered. In order to include some relativistic effects, the solution to the SE can be replaced by the large component of the solution to the scalar-relativistic Schrödinger equation (A.20). An extensive derivation of it can be found in Appendix A. A way to include spin-orbit effects as well is described in Section 2.6.

With the construction of the described basis, the Kohn-Sham equations take the form of a generalized eigenvalue problem resulting in the secular equation

$$H^{\boldsymbol{k}} C^{\boldsymbol{k}} = \epsilon^{\boldsymbol{k}} S^{\boldsymbol{k}} C^{\boldsymbol{k}}, \tag{2.7}$$

with matrix elements

$$H^{\boldsymbol{k}}_{GG'} = \langle \phi_{G+\boldsymbol{k}} | -\frac{1}{2}\nabla^2 + v_{KS}(\boldsymbol{r}) | \phi_{G+\boldsymbol{k}} \rangle \tag{2.8}$$

and

$$S^{\boldsymbol{k}}_{GG'} = \langle \phi_{G+\boldsymbol{k}} | \phi_{G'+\boldsymbol{k}} \rangle . \tag{2.9}$$

$C^{\boldsymbol{k}}$ represents the coefficients defined in the wavefunction expansion Eq. (2.4).
Although the solution to this problem seems to be quite easy on the first glance, it is complicated in practice. If one takes a closer look, one can see that the basis functions and to be more specific — the solutions of the radial SE depend on $\epsilon_{i\boldsymbol{k}}$. Thus the secular equation (2.7) is not linear in energy. Since it would be a much more computational demanding task to solve such a non linear equation, we have to find a way to linearize the secular equation (2.7) first. One way is to take a fixed energy parameter $\epsilon_{l\alpha}$ in the radial Schrödinger equation (2.6), the secular equation would remain linear and the solution would be rather simple. Unfortunately, this does not lead to reasonable results and is not used in practice.

Since this is no satisfactory solution for the linearization problem, a series of more workable methods have been developed. With one of the most popular ones being the linearized augmented planewave (LAPW) method.

2.3. Linearized Augmented Planewaves

To avoid the need for solving the non-linear secular equation (2.7), Anderson proposed in 1975 [9] the LAPW method. In order to minimize the error introduced through a fixed energy parameter in the radial SE, he suggested to expand the radial functions $u_{l\alpha}(r)$ in a way similar to a Taylor expansion around the fixed energy parameter ϵ_{la}

$$u_{l\alpha}(r_\alpha) \approx u_{l\alpha}(r_\alpha; \epsilon_{l\alpha}) + (\epsilon - \epsilon_{l\alpha})\dot{u}_{l\alpha}(r_\alpha; \epsilon_{l\alpha}), \tag{2.10}$$

with $\dot{u}_{l\alpha}$ being the energy derivative of the radial function. This leads to a second order error in the radial function and therefore, to an error of fourth order in energy.

The Equation (2.10) can then be substituted into the definition of the APW basis set Eq. (2.5). That results in a new basis definition:

$$\phi_{G+\boldsymbol{k}}(\boldsymbol{r}) = \begin{cases} \sum_{lm}[A^{G+\boldsymbol{k}}_{lm\alpha} u_{l\alpha}(r_\alpha; \epsilon_{l\alpha}) + B^{G+\boldsymbol{k}}_{lm\alpha} \dot{u}_{l\alpha}(r_\alpha; \epsilon_{l\alpha})]Y_{lm}(\hat{\boldsymbol{r}}_\alpha), & r_\alpha \leq R_{MT} \\ \frac{1}{\sqrt{\Omega}} e^{i(G+\boldsymbol{k})\boldsymbol{r}}, & \boldsymbol{r} \in I, \end{cases} \tag{2.11}$$

where $A^{G+\boldsymbol{k}}_{lm\alpha}$ and $B^{G+\boldsymbol{k}}_{lm\alpha}$ are coefficients that allow for the basis functions as well as its first radial derivative to be continuous at the MT-boundary. Although this approach is an improvement over the APW method with fixed energy parameters, it does not ensure a sufficiently small linearization error. To further minimize the linearization error, local orbitals can be added to the basis.

2.4. Local Orbitals

If local orbitals are included in the basis, the KS-orbitals take the form

$$\psi_{i\boldsymbol{k}}(\boldsymbol{r}) = \sum_G C^{\boldsymbol{k}}_{iG} \phi_{G+\boldsymbol{k}}(\boldsymbol{r}) + \sum_\mu C^{\boldsymbol{k}}_{i\mu} \phi_\mu(\boldsymbol{r}), \tag{2.12}$$

with μ being an index running over all local orbitals

$$\phi_\mu(\boldsymbol{r}) = \begin{cases} \delta_{\alpha\alpha_\mu}\delta_{ll_\mu}\delta_{mm_\mu}[a_\mu u_{l\alpha}(r_\alpha; \epsilon_{l\alpha}) + b_\mu \dot{u}_{l\alpha}(r_\alpha; \epsilon_{l\alpha})]Y_{lm}(\hat{r}_\alpha), & r_\alpha \leq R_{MT} \\ 0, & \boldsymbol{r} \in I. \end{cases} \tag{2.13}$$

This kind of basis function is zero in the interstitial region. The coefficients are chosen such that the function is continuous at the MT-boundary and normalized to one. As the LAPWs, the LOs include the energy derivative $\dot{u}_{l\alpha}(r_\alpha; \epsilon_{l\alpha})$. This increases the flexibility of the basis and therefore allows one to use fixed energy parameters in the APW basis set.

LOs in contrast to LAPWs have to follow fewer restrictions. They have to only match the value of the basis function at the MT boundary instead of matching the slope, as well. Due to the higher flexibility of the LOs and the fact, that they do not need to describe the interstitial region, fewer basis function are needed in the APW+LO basis than in the LAPW basis, while keeping the linearization errors in the same order.

2.5. Wigner-Seitz Rules

In order to minimize the linearization error, the linearization energy $\epsilon_{l\alpha}$ should be set as close as possible to the solution to the KS equations. Since there is not one basis set for each $\boldsymbol{k}$-point, we have to find a compromise that fits all $\boldsymbol{k}$-points. Hence there is no direct relation between the linearization energy $\epsilon_{l\alpha}$ and the KS eigenvalues $\epsilon_{i\boldsymbol{k}}$. The KS eigenvalues depend on the band index as well as the $\boldsymbol{k}$-point whereas the linearization energies are independent from $\boldsymbol{k}$. To be able to map between the linearization energies and the KS eigenvalues, one has to choose one specific $\boldsymbol{k}$-point for every band.

There are different methods how the linearization energy can be chosen. The one that we use in this work is an empirical method which follows the Wigner-Seitz rules [10]. These rules state, that the ideal linearization energy for a band with predominantly l-character can be found between the energy for which the wavefunction itself is zero at the MT-radius

$$u_{l\alpha}(r_\alpha, E_{\max})\Big|_{r_\alpha = R_{MT}} = 0 \tag{2.14}$$

and the energy were the first derivative with respect to r is zero at the MT-boundary

$$\frac{\partial u_{l\alpha}(r_\alpha, E_{\min})}{\partial r_\alpha}\Big|_{r_\alpha = R_{MT}} = 0. \tag{2.15}$$

We then choose the linearization energy to be the mean of these two boundary values

$$\epsilon_{l\alpha} = \frac{E_{\max} + E_{\min}}{2}. \tag{2.16}$$

2.6. Spin-Orbit Coupling

Until now we considered only scalar relativistic effects. The secular equation as well as the equation for modeling the basis functions, therefore, do not include spin-orbit coupling — a property which can be important especially for materials containing heavier elements. To consider SOC, we need to solve the full Dirac equation instead of the scalar relativistic Schrödinger equation. Due to the fact that the SOC term couples spin-up and spin-down wavefunctions, the size of the secular equation then increases from $\widetilde{N} \times \widetilde{N}$ (with $\widetilde{N}$ being the number of basis functions) to $2\widetilde{N} \times 2\widetilde{N}$. Since the computing time scales cubically, we end up with an eight times higher time demand.

To avoid the difficulty of this fully relativistic approach one can make use of the fact that SOC is in most cases only a small effect. The so called second-variational approach uses the standard scalar relativistic LAPW+LO basis as a starting point to build and solve a secular equation. In this first step, SOC effects are completely neglected. After solving the first secular equation, only the lowest N scalar relativistic orbitals that are relevant for SOC are used to set up a second secular equation, which now contains the fully relativistic Hamiltonian. But since the number of relevant bands N is in most cases much smaller than the total number of basis functions $\widetilde{N}$, the computational cost remains relatively small. The

new secular equation can then be solved. This whole procedure, is done for every $\boldsymbol{k}$-point and every self-consistent loop. This second-variational approach leads to mostly good results even for a relatively small number of included bands. However, there are some cases where calculations do not converge well with respect to N, when this method is used. As shown by Nordström et al. [11] this approach can also lead to problems in the calculation of total energies and related equilibrium lattice constants of actinide elements. This finding can be extended to heavy elements containing valence orbitals with p-character in general [12].

In `exciting` a slightly different approach is implemented (C. Draxl, A. Gulans, S.Lubeck, C. Vona, to be published). Not only the lowest bands are used to form the secular equation, but in addition all LOs from the original basis. To avoid linear dependencies, the LO components in the orbitals used in the new basis have been eliminated. The resulting basis set is still small enough to remain within reasonable computing times.

In spite of these extra orbitals, the before mentioned issues concerning heavy p-elements remain. The problems result from the fact, that fully relativistic properties are described in a scalar relativistic basis set or more precisely, from the poor description of the $p_{1/2}$ orbitals in the basis, where the subscript 1/2 stands for the total angular momentum quantum number j. Despite $p_{3/2}$ orbitals take a quite similar form as the scalar relativistic p orbitals, $p_{1/2}$ have a different behavior close to $r = 0$. As shown in Fig. 2.1, the orbitals take a non-zero value at $r = 0$ and therefore, can not be described by a scalar relativistic basis.

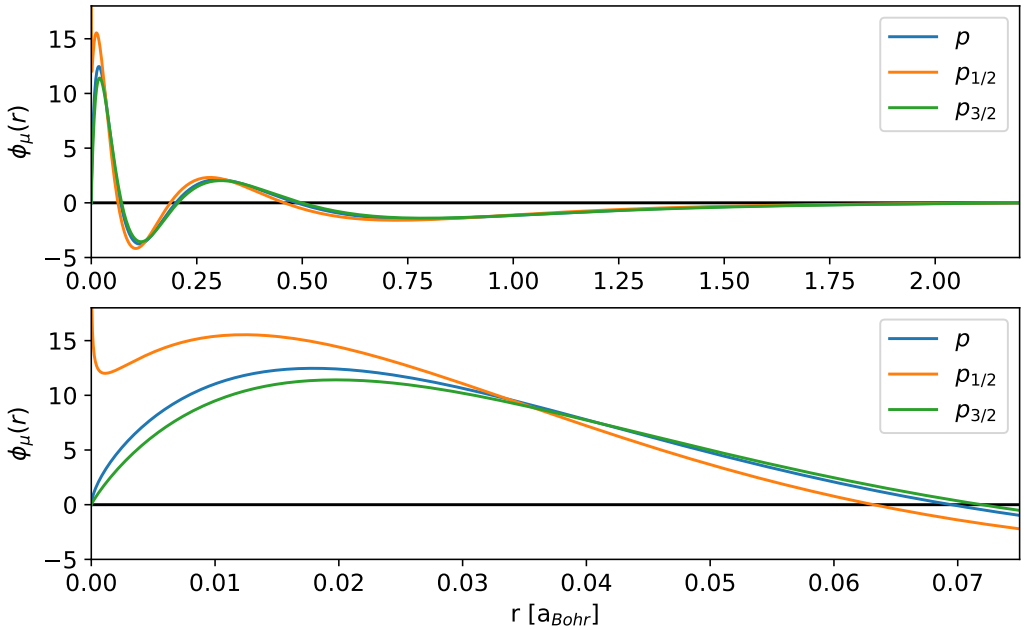

Figure 2.1.: Comparison of $p_{1/2}$, $p_{3/2}$, and p local orbitals in Pb showing the large differences between the relativistic and the non-relativistic basis functions.

In order to describe all states properly, Kuneš et al. proposed to add special $p_{1/2}$ local orbitals to the second-variational basis [13]. These new local orbitals are build from wave functions that depend on the total angular momentum quantum number j. We obtain them by solving the radial Dirac equation (A.19). A more extensive derivation of it can be found in Appendix A. We show in this work a slightly different approach, where fully relativistic local orbitals are added not only to the second-variational basis, but also to the original basis set.

3. Computation of Linearization Energies

3.1. Implementation of Wigner-Seitz Rules

Linearization energies in `exciting` are explicit input parameters, which need to be chosen manually. Due to that, calculated results can vary according to differences in the choice of linearization energies.

In order to get reasonable values for the linearization energies and to avoid variations in the results, we implement the Wigner-Seitz rules as described in Section 2.5. This scheme allows one in practice to provide only the number of nodes N_{nodes} of the desired wave function as input. The linearization energy is then computed from it. The number of nodes is in contrast to linearization energies fixed for every orbital. It can be calculated from the principal quantum number n and the azimuthal quantum number l

$$N_{\text{nodes}} = n - l - 1. \tag{3.1}$$

N_{nodes} determines two bounds for possible linearization energies. The upper bound energy E_{upper} can be calculated by finding a wave function that solves the Schrödinger equation (A.20), has got the correct number of nodes, and vanishes at the MT boundary. The lower bound E_{lower} is then given by the the wave function that solves the Schrödinger equation, again vanishes at the MT boundary, but has got one node less. In between these two bounds, the linearization energy can be found. With the help of the Wigner-Seitz rules the lower bound can be further tightened. Therefore, we search for the energy for which the radial derivative of the wave function vanishes at the MT boundary. This is done by using the bisection method, where E_{upper} and E_{lower} serve as the starting values. To get the actual linearization energy, we take the mean of the upper bound energy and the energy calculated in the bisection.

$$\epsilon_{l\alpha} = \frac{E_{\text{upper}} + E_{\text{bisection}}}{2}. \tag{3.2}$$

3.2. Delta-DFT Method

In order to test how well computed linearization energies work in contrast to linearization energies chosen manually, we want to cover a big range of different materials. Therefore, we use an existing set of test cases. The applied method was developed in order to pairwise compare different DFT codes [14]. The so-called Δ-gauge is a way to condense differences between two equations of state (EOS) into a single value. In order to get this value, the total energy of a material is determined for volumes in the interval around the equilibrium volume V_0 reaching from $V_0 - 6\%$ to $V_0 + 6\%$. These EOS are computed for calculations of the two

DFT-codes (a and b) to be compared. The root-mean-square difference of these two curves is then called the Δ-gauge

$$\Delta_i(a,b) = \sqrt{\frac{\int_{0.94V_0}^{1.06V_0}(E_{bi}(V) - E_{ai}(V))^2 dV}{0.12V_0}}. \tag{3.3}$$

In Ref. [14], it is proposed to calculate Δ-values Δ_i for a benchmark set of 71 elemental crystals i. The average of these Δ_i is then taken as a representation for the discrepancy between two DFT codes. In order to get some reference Δ-values, they compared different experimental EOS and obtained an average Δ_{exp} of about 1.0 meV/atom. The average Δ of independent DFT codes is about 0.8 meV/atom. The smallest Δ they got between two independent codes is quoted as 0.1 meV/atom.

In this work, we do not compare two different DFT codes, instead, we compare calculations where the linearization energies are optimized manually with calculations where the linearization energies are computed automatically. All calculations are executed with the computer package `exciting`. For the manually optimized calculations, we use the values from Ref. [14]. We consider a subset of 66 elemental crystals and obtain the largest Δ-value for polonium ($2.13 \cdot 10^{-2}$ meV/atom). The majority of Δ-values is smaller than 10^{-6} meV/atom. All Δ-values can be found in Appendix B (Tab. B.1). These Δ-values can be considered as extremely small and show that the automated determination of linearization energies is sufficient to achieve results very close to the results computed with manually optimized linearization energies of benchmark quality.

4. Generation of j-dependent Local Orbitals

4.1. Implementation of j-dependent Local Orbitals

As mentioned in Section 2.6, it is necessary to include $p_{1/2}$ local orbitals in the basis in order to sufficiently capture spin-orbit-coupling effects. We use wavefunctions that solve the radial Dirac equation (A.19) to build these j-dependent LOs. For the purpose of going from l-dependent to j-dependent LOs, we exchange the solver for the scalar relativistic Schrödinger equation (A.20) with a solver for the radial Dirac equation. Such a solver was already implemented in `exciting`. It integrates the radial Dirac equation for a given spherically symmetric potential, principal quantum number n, azimuthal quantum number l, and relativistic quantum number κ from $r = 0$ outwards.

On the first glance, the radial Dirac equation and therefore the wavefunctions do not depend on the total angular momentum quantum number j anymore, however there is a direct relation between κ and j

$$\kappa = \begin{cases} -l-1, & j = l + \frac{1}{2} \\ l, & j = l - \frac{1}{2} \end{cases}. \tag{4.1}$$

For $l = 0$ only -1 is a valid choice for κ. To simplify the radial Dirac equation, κ instead of j is used.

4.2. Computations of PbI_2 and $CsPbI_3$

We chose lead iodide (PbI_2) and cesium lead iodide ($CsPbI_3$) as materials to evaluate the impact of j-dependent LOs. Lead (Pb) belongs to the group of heavy elements containing valence p-orbitals. We therefore, expect a strong impact of SOC and especially an influence of $p_{1/2}$ orbitals in the basis. All calculations are performed with three different methods implemented in `exciting`. The first method is an implementation of the second-variational approach with scalar relativistic local orbitals included in the second-variational basis as described in Section 2.6. In the second method, we add j-dependent LOs to the basis as described in Section 2.6 as well. The third approach is a fully relativistic implementation of SOC in `exciting`. The latter method is taken as reference. All calculations are performed using the Perdew-Burke-Ernzerhof (PBE) functional [15].

We compare the convergence of different properties with respect to the number of basis functions N_{bf}. This comparison is done for the second-variational approach with and without j-dependent local orbitals. The LOs we used, can be found in Tab. C.1 in Appendix C.

As shown in Fig. 4.1 the fundamental band gaps E_{gap} of PbI_2 calculated without j-dependent local orbitals on the one hand converges faster. However, it does not approach the band gap obtained by the fully relativistic implementation, as indicated in Tab. 4.1. The results from the second-variational method with j-dependent local orbitals on the other hand converge more slowly, but come closer to the fully relativistic results. The same applies for the convergence of the total energy E_{tot} and the spin-orbit-splitting of the lowest unoccupied state at $\boldsymbol{k}$-point K, E_{so}. Plots of the convergence behavior can be found in Appendix C.

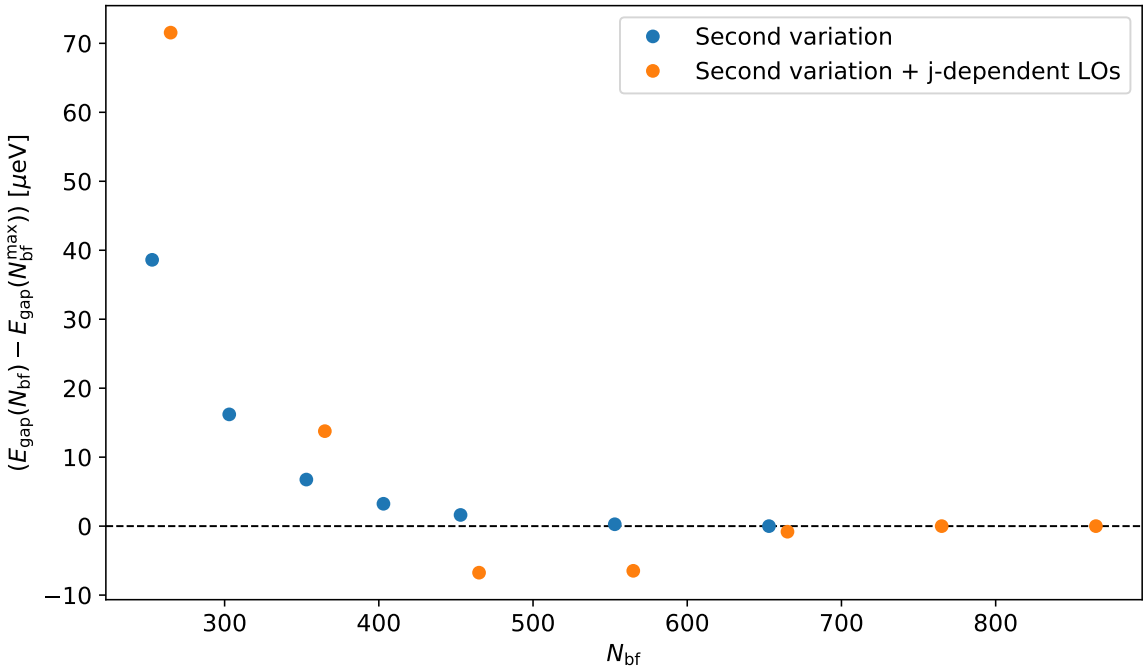

Figure 4.1.: Convergence of the computed PbI_2 band gaps with respect to the number of basis functions. The zero energy is set to the converged value.

	Second variation	Second variation + j-dependent LOs	Fully relativistic
E_{tot} [Ha]	-35166.597060	-35167.089266	-35167.078055
E_{gap} [eV]	1.624	1.367	1.365
E_{so} [eV]	0.7739	1.0182	1.0187

Table 4.1.: Comparison of converged values of the total energy E_{tot}, fundamental band gap E_{gap}, and spin-orbit-splitting E_{so} of the lowest unoccupied state at $\boldsymbol{k}$-point K computed for PbI_2 with the three SOC implementations in `exciting`.

The same analysis is done for $CsPbI_3$. As demonstrated in Fig. 4.2, it leads to similar results. Again the calculations performed by the version without j-dependent local orbitals converge faster, but do not approach the results from the fully relativistic reference (Table: 4.2), whereas the converged results computed with j-dependent LOs reproduce the results of the fully relativistic version better. Convergence tests for the total energy and the spin-orbit-splitting of the lowest unoccupied state at the k-point M can be found in the Appendix C.

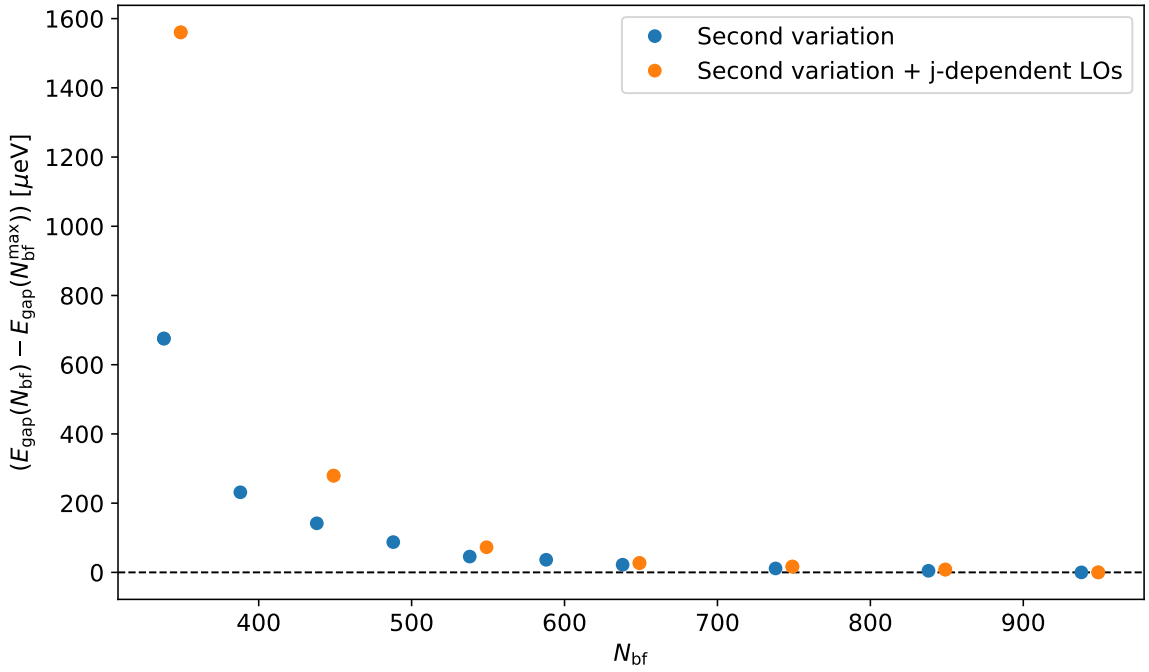

Figure 4.2.: Convergence of the computed $CsPbI_3$ band gaps with respect to the number of basis functions. The zero energy is set to the converged value.

	Second variation	Second variation + j-dependent LOs	Fully relativistic
E_{tot} [Ha]	-50076.025923	-50076.622527	-50076.608860
E_{gap} [eV]	0.602	0.022	0.021
E_{so} [eV]	0.983	1.231	1.232

Table 4.2.: Comparison of converged values of the total energy E_{tot}, fundamental band gap E_{gap}, and spin-orbit-splitting E_{so} of the lowest unoccupied state at $\boldsymbol{k}$-point M computed for $CsPbI_3$ with the three SOC implementations in `exciting`.

5. Conclusion

5.1. Computation of Linearization Energies

As shown in Section 3.2, automatically generated linearization energies lead to results very close to solutions obtained with manually optimized linearization energies. Thus, it is not necessary to give linearization energies as an explicit input parameter.

Optimization of linearization energies by hand is very time-consuming, since the same calculation needs to be repeated for several different sets of linearization energies to find the set that minimizes the total energy of a system. With the Wigner-Seitz algorithm, the calculation needs to be performed only ones. In addition to that, the linearization energies are material dependent. The material dependence of the input gets reduced with the introduction of automatically calculated linearization energies. So it is easier to generate input for new materials. This is a big advantage for the generation of input for high-throughput calculations. It also leads in general to a better reproducibility of calculations.

Although the results are close to the manually obtained results, there still are slight differences. To further reduce these differences, one could investigate the mixing parameter. The Wigner-Seitz rules include a parameter a_{mix} for the mixing between the two energies E_{max} and E_{min}.

$$\epsilon_{l\alpha} = a_{\text{mix}} \cdot E_{\text{max}} + (1 - a_{\text{mix}}) \cdot E_{\text{min}}. \tag{5.1}$$

We chose this parameter to be 1/2. In order to find out if this is the best choice, further calculations with different a_{mix} could be performed.

5.2. Second Variation with j-dependent Local Orbitals

The integration of j-dependent local orbitals to the second-variational basis leads to a better agreement with the results of fully relativistic reference calculations. Whereby the Hamiltonian size increases only slightly. Therefore, we get a better description of SOC effects, but stay within relatively small computation times compared to the fully relativistic reference. We got a better agreement with the reference even for relatively small numbers of basis functions. This simplifies the investigation of materials with for example heavy elements as lead.

In this work, we used only one set of additional j-dependent local orbitals for each material. In order to find out which local orbitals are specifically important, the performed calculations could be repeated for different sets of local orbitals.

Bibliography

1. GULANS, A. et al.: Exciting: a full-potential all-electron package implementing density-functional theory and many-body perturbation theory. *Journal of Physics: Condensed Matter*. 2014, vol. 26, no. 36, p. 363202.
2. EVEN, J. et al.: Importance of spin–orbit coupling in hybrid organic/inorganic perovskites for photovoltaic applications. *The Journal of Physical Chemistry Letters*. 2013, vol. 4, no. 17, pp. 2999–3005.
3. HOHENBERG, P.; KOHN, W.: Inhomogeneous electron gas. *Physical review*. 1964, vol. 136, no. 3B, B864.
4. KOHN, W.; SHAM, L. J.: Self-consistent equations including exchange and correlation effects. *Physical review*. 1965, vol. 140, no. 4A, A1133.
5. VON BARTH, U.; HEDIN, L.: A local exchange-correlation potential for the spin polarized case. i. *Journal of Physics C: Solid State Physics*. 1972, vol. 5, no. 13, p. 1629.
6. PERDEW, J. P. et al.: Generalized gradient approximation made simple. *Physical review letters*. 1996, vol. 77, no. 18, p. 3865.
7. MATSUSHITA, Y.-i. et al.: Comparative study of hybrid functionals applied to structural and electronic properties of semiconductors and insulators. *Physical Review B*. 2011, vol. 84, no. 7, p. 075205.
8. SLATER, J. C.: Wave functions in a periodic potential. *Physical Review*. 1937, vol. 51, no. 10, p. 846.
9. ANDERSEN, O. K.: Linear methods in band theory. *Physical Review B*. 1975, vol. 12, no. 8, p. 3060.
10. ANDERSEN, O.: Simple approach to the band-structure problem. *Solid State Communications*. 1973, vol. 13, no. 2, pp. 133–136.
11. NORDSTRÖM, L. et al.: Spin-orbit coupling in the actinide elements: A critical evaluation of theoretical equilibrium volumes. *Physical Review B*. 2000, vol. 63, no. 3, p. 035103.
12. HUHN, W. P.; BLUM, V.: One-hundred-three compound band-structure benchmark of post-self-consistent spin-orbit coupling treatments in density functional theory. *Physical Review Materials*. 2017, vol. 1, no. 3, p. 033803.
13. KUNEŠ, J. et al.: Electronic structure of fcc Th: Spin-orbit calculation with 6 p 1/2 local orbital extension. *Physical Review B*. 2001, vol. 64, no. 15, p. 153102.
14. LEJAEGHERE, K. et al.: Reproducibility in density functional theory calculations of solids. *Science*. 2016, vol. 351, no. 6280.
15. PERDEW, J. et al.: Perdew, burke, and ernzerhof reply. *Physical Review Letters*. 1998, vol. 80, no. 4, p. 891.

16. BLOMQUIST, E.; BOMAN, T.: *The Dirac equation for a particle in a spherical box potential with application in bag modeling*. 2015.

17. SINGH, D. J.; NORDSTROM, L.: Planewaves, Pseudopotentials, and the LAPW method. *Springer Science & Business Media*. 2006.

List of Figures

List of Tables

Appendix

A. Dirac-Equation

The following derivation is based on Ref. [16] and Ref. [17]. In order to consider relativistic effects, the Dirac equation serves as an alternative to the non-relativistic Schrödinger equation. Starting from the general four component Dirac equation we derive the radial Dirac equation and show how the SOC contribution can be separated to get a simplified scalar relativistic equation.

The four component Dirac equation takes the following form

$$H_D \Psi = \epsilon \Psi \tag{A.1}$$

with

$$H_D = \begin{pmatrix} V & c(\boldsymbol{\sigma p}) \\ c(\boldsymbol{\sigma p}) & V - 2mc^2 \end{pmatrix} \tag{A.2}$$

and

$$\Psi = \begin{pmatrix} \psi_\alpha \\ \psi_\beta \\ \phi_\alpha \\ \phi_\beta \end{pmatrix}, \tag{A.3}$$

where ψ_i are the large components and ϕ_i the small components of the wavefunction. $\boldsymbol{p}$ is the three dimensional momentum operator

$$\boldsymbol{p} = -i\nabla \tag{A.4}$$

and σ is a vector consisting of the Pauli matrices σ_i

$$\boldsymbol{\sigma} = \begin{pmatrix} \sigma_x \\ \sigma_y \\ \sigma_z \end{pmatrix}, \tag{A.5}$$

with $\boldsymbol{\sigma_i}$ being

$$\sigma_x = \begin{pmatrix} 0 & 1 \\ 1 & 0 \end{pmatrix} \quad \text{(A.6a)} \qquad \sigma_x = \begin{pmatrix} 0 & -i \\ i & 0 \end{pmatrix} \quad \text{(A.6b)} \qquad \sigma_x = \begin{pmatrix} 1 & 0 \\ 0 & -1 \end{pmatrix}. \quad \text{(A.6c)}$$

By decoupling the Dirac equation into two equations each containing either the small or large component of the wavefunction

$$\phi = (\epsilon + 2m - V)^{-1}(\boldsymbol{\sigma p})\phi \tag{A.7a}$$

$$\frac{1}{2}(\boldsymbol{\sigma p})\left(1+\frac{\epsilon-V}{2m}\right)^{-1}(\boldsymbol{\sigma p})\psi + V\psi = \epsilon\psi \tag{A.7b}$$

the kinetic energy operator K can be defined as

$$\left(1+\frac{\epsilon-V}{2m}\right)^{-1} = K. \tag{A.8}$$

Therefore, we end up with the following Dirac equation for the large component

$$\frac{1}{2}(\boldsymbol{\sigma p})K(\boldsymbol{\sigma p})\psi + V\psi = \epsilon\psi. \tag{A.9}$$

With the help of some algebra we can split the kinetic energy term into a scalar relativistic term and a spin-orbit term:

$$\begin{aligned}
\frac{1}{2}(\boldsymbol{\sigma p})K(\boldsymbol{\sigma p}) &= \frac{1}{2}\begin{pmatrix} p_z & p_x - ip_y \\ p_x + ip_y & -p_z \end{pmatrix} K \begin{pmatrix} p_z & p_x - ip_y \\ p_x + ip_y & -p_z \end{pmatrix} \\
&= \frac{1}{2}\begin{pmatrix} p_z K p_z + (p_x - ip_y)K(p_x + ip_y) & p_z K(p_x - ip_y) - (p_x - ip_y)K p_z \\ (p_x + ip_y)K p_z - p_z K(p_x + ip_y) & (p_x + ip_y)K(p_x - ip_y) + p_z K p_z \end{pmatrix} \\
&= \frac{1}{2}\begin{pmatrix} \boldsymbol{p}K\boldsymbol{p} & 0 \\ 0 & \boldsymbol{p}K\boldsymbol{p} \end{pmatrix} + \frac{1}{2}\begin{pmatrix} i(p_x K p_y - p_y K p_x) & p_z K(p_x - ip_y) - (p_x - ip_y)K p_z \\ -p_z k(p_x + ip_y) + (p_x + ip_y)K p_z & -i(p_x K p_y + p_y K p_x) \end{pmatrix} \\
&= \frac{1}{2}\mathbb{I}\boldsymbol{p}K\boldsymbol{p} + \frac{i}{2}\boldsymbol{\sigma}((\boldsymbol{p}K)\times\boldsymbol{p}),
\end{aligned} \tag{A.10}$$

where the first term $\frac{1}{2}\mathbb{I}\boldsymbol{p}K\boldsymbol{p}$ is the scalar-relativistic contribution and the second term $\frac{i}{2}\boldsymbol{\sigma}((\boldsymbol{p}K)\times\boldsymbol{p})$ is the SOC contribution. This gets clearer by inserting the expressions for $\boldsymbol{p}$, Eq. (A.4), and K, Eq. (A.8),

$$\hat{T} = \frac{1}{2}\mathbb{I}\boldsymbol{p}K\boldsymbol{p} + \frac{i}{2}\boldsymbol{\sigma}((\boldsymbol{p}K)\times\boldsymbol{p}) = -\frac{1}{2}\nabla\frac{1}{1+\frac{\epsilon-V}{2}}\nabla - \frac{i}{2}\boldsymbol{\sigma}\left(\nabla\frac{1}{1+\frac{\epsilon-V}{2}}\times\nabla\right) \tag{A.11}$$

and simplifying it by applying the chain and product rule for the derivation

$$\hat{T} = -\frac{1}{2}\nabla\frac{1}{1+\frac{\epsilon-V}{2}}\nabla - \frac{i}{4\left(1+\frac{\epsilon-V}{2}\right)^2}\boldsymbol{\sigma}(\nabla V\times\nabla). \tag{A.12}$$

When assuming the potential V to be a central potential $V(r)$, SOC gets easily visible

$$\begin{aligned}
-i\boldsymbol{\sigma}(\nabla V\times\nabla) &= -\frac{i}{r}\frac{\partial V}{\partial r}\boldsymbol{\sigma}(\boldsymbol{r}\times\nabla) \\
&= \frac{1}{r}\frac{\partial V}{\partial r}\boldsymbol{\sigma}(\boldsymbol{r}\times\boldsymbol{p}) \\
&= \frac{1}{r}\frac{\partial V}{\partial r}\boldsymbol{\sigma}\boldsymbol{L}
\end{aligned} \tag{A.13}$$

$$\Longrightarrow \hat{T} = -\frac{1}{2}\nabla\frac{1}{1+\frac{\epsilon-V}{2}}\nabla + \frac{1}{4\left(1+\frac{\epsilon-V}{2}\right)^2}\frac{1}{r}\frac{V}{r}\boldsymbol{\sigma L} \tag{A.14}$$

where $\boldsymbol{\sigma}$ represents the spin and $\boldsymbol{L}$ the orbit component.

Similar to the derivation of the radial Schrödinger equation, we can develop a radial Dirac equation for particles in a central potential. In order to reach that we will step back and start again with the four-component Dirac equation. We introduce the operator $\hat{K}_2$ which is defined as

$$\hat{K}_2 = \boldsymbol{\sigma L} + 1. \tag{A.15}$$

Its eigenvalues therefore are

$$\kappa = \begin{cases} -l-1, & j = l+\frac{1}{2} \\ l, & j = l-\frac{1}{2} \end{cases}. \tag{A.16}$$

The solution of the Dirac equation can be written as a product ansatz

$$\psi_\kappa = \begin{pmatrix} g_\kappa(r)\chi_\kappa^m \\ -if_\kappa(r)\chi_{-\kappa}^m \end{pmatrix}, \tag{A.17}$$

where κ is the relativistic quantum number and χ_κ^m is a two-component spinor. If we now plug the ansatz into the Dirac equation we end up with the radial Dirac equation:

$$\frac{\partial f_\kappa}{\partial r} = \frac{1}{c}(V-E)g_\kappa + \frac{\kappa-1}{r}f_\kappa \tag{A.18a}$$

$$\frac{\partial g_\kappa}{\partial r} = -\frac{\kappa-1}{r}g_\kappa + 2\left(1+\frac{E-V}{2mc^2}\right)cf_\kappa. \tag{A.18b}$$

Now we can again eliminate the small component and distinguish between scalar relativistic and SOC components

$$-\frac{1}{2(1+\frac{E-V}{2mc^2})}\left(g_\kappa'' + \frac{2}{r}g_\kappa' - \frac{l(l+1)}{r^2}g_\kappa\right) - \frac{V'g_\kappa'}{4(1+\frac{E-V}{2mc^2})^2c^2} - \frac{\kappa+1}{r}\frac{V'g_\kappa}{4(1+\frac{E-V}{2mc^2})^2c^2} + Vg_\kappa = Eg_\kappa. \tag{A.19}$$

The first term is the scalar-relativistic one, the second one is the SOC. In order to get the scalar-relativistic Schrödinger equation, the SOC term is neglected

$$-\frac{1}{2(1+\frac{E-V}{2mc^2})}\left(g_\kappa'' + \frac{2}{r}g_\kappa' - \frac{l(l+1)}{r^2}g_\kappa\right) - \frac{V'g_\kappa'}{4(1+\frac{E-V}{2mc^2})^2c^2} + Vg_\kappa = Eg_\kappa. \tag{A.20}$$

B. Delta-DFT

Element	Δ_i [meV/atom]	Element	Δ_i [meV/atom]	Element	Δ_i [meV/atom]
He	0	Cr	0	In	$2.858 \cdot 10^{-4}$
Li	0	Mn	$8.184 \cdot 10^{-6}$	Sn	0
Be	0	Co	$1.147 \cdot 10^{-2}$	Sb	0
B	0	Zn	0	Te	$2.679 \cdot 10^{-3}$
C	0	Cu	0	I	0
N	0	Ga	0	Xe	$5.731 \cdot 10^{-4}$
O	0	Ge	0	Cs	0
F	0	As	0	Ba	$8.864 \cdot 10^{-4}$
Ne	0	Se	0	Lu	$7.371 \cdot 10^{-4}$
Na	0	Kr	0	Hf	$3.038 \cdot 10^{-4}$
Mg	0	Rb	0	Ta	$3.961 \cdot 10^{-3}$
Al	0	Sr	$7.141 \cdot 10^{-4}$	W	$2.450 \cdot 10^{-3}$
Si	0	Y	0	R	0
P	0	Zr	$4.969 \cdot 10^{-5}$	Os	$8.884 \cdot 10^{-4}$
S	0	Nb	0	Ir	0
Cl	0	Mo	0	Pt	$2.298 \cdot 10^{-3}$
Ar	0	Tc	0	Au	$6.578 \cdot 10^{-3}$
K	$7.466 \cdot 10^{-06}$	Ru	$1.260 \cdot 10^{-5}$	Hg	$2.104 \cdot 10^{-3}$
Ca	0	Rh	$3.439 \cdot 10^{-4}$	Tl	0
Sc	0	Pd	$3.594 \cdot 10^{-4}$	Pb	$7.149 \cdot 10^{-4}$
Ti	0	Ag	$2.369 \cdot 10^{-4}$	Bi	0
V	0	Cd	0	Po	$2.130 \cdot 10^{-2}$

Table B.1.: Δ-values for 66 elemental crystals. Values smaller than 10^{-6} are indicated as zero.

C. j-Dependent Local Orbitals

Material	Element	second variation	second variation + j-dependent LOs
PbI_2	Pb	$4 \times p$	$2 \times p_{3/2}$ $1 \times p_{1/2}$ $1 \times$ mixed $p_{1/2}$ & $p_{3/2}$
	I	$3 \times p$	$2 \times p_{3/2}$ $1 \times p_{1/2}$ $2 \times$ mixed $p_{1/2}$ & $p_{3/2}$
$CsPbI_3$	Cs	$4 \times p$	$3 \times p_{3/2}$ $1 \times p_{1/2}$ $1 \times$ mixed $p_{1/2}$ & $p_{3/2}$
	Pb	$4 \times p$	$2 \times p_{3/2}$ $1 \times p_{1/2}$ $1 \times$ mixed $p_{1/2}$ & $p_{3/2}$
	I	$3 \times p$	$3 \times p_{3/2}$ $1 \times p_{1/2}$ $1 \times$ mixed $p_{1/2}$ & $p_{3/2}$

Table C.1.: p orbitals included in the second-variational basis with and without j-dependent local orbitals.

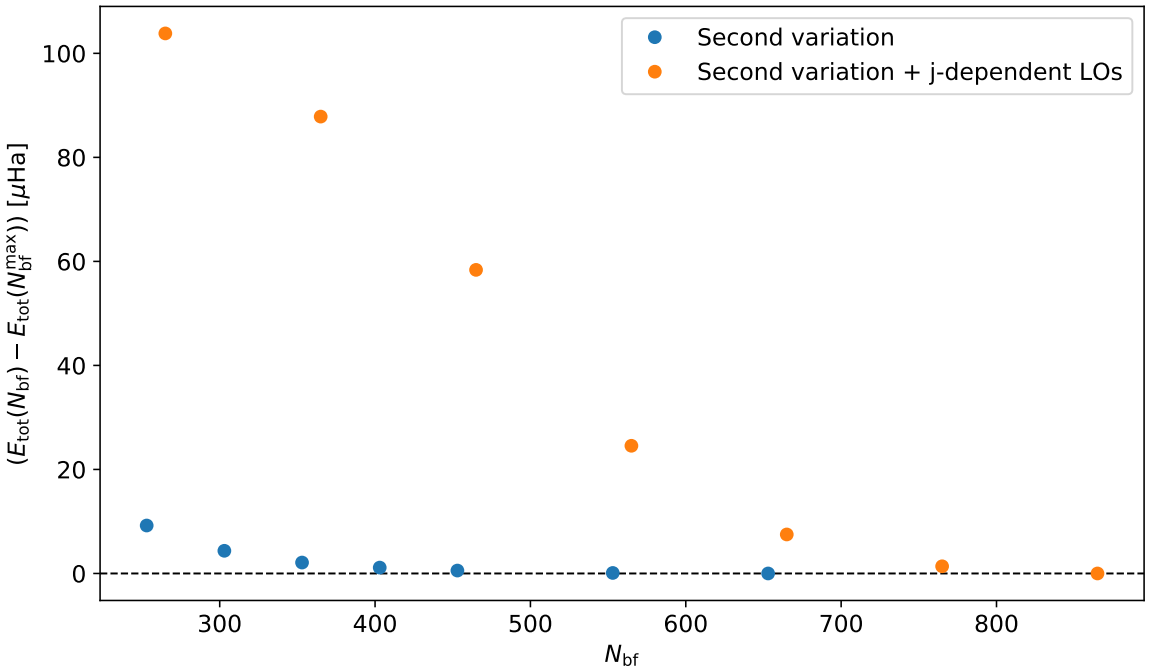

Figure C.1.: Convergence of the computed PbI_2 total energies with respect to the number of basis functions. The zero energy is set to the converged value.

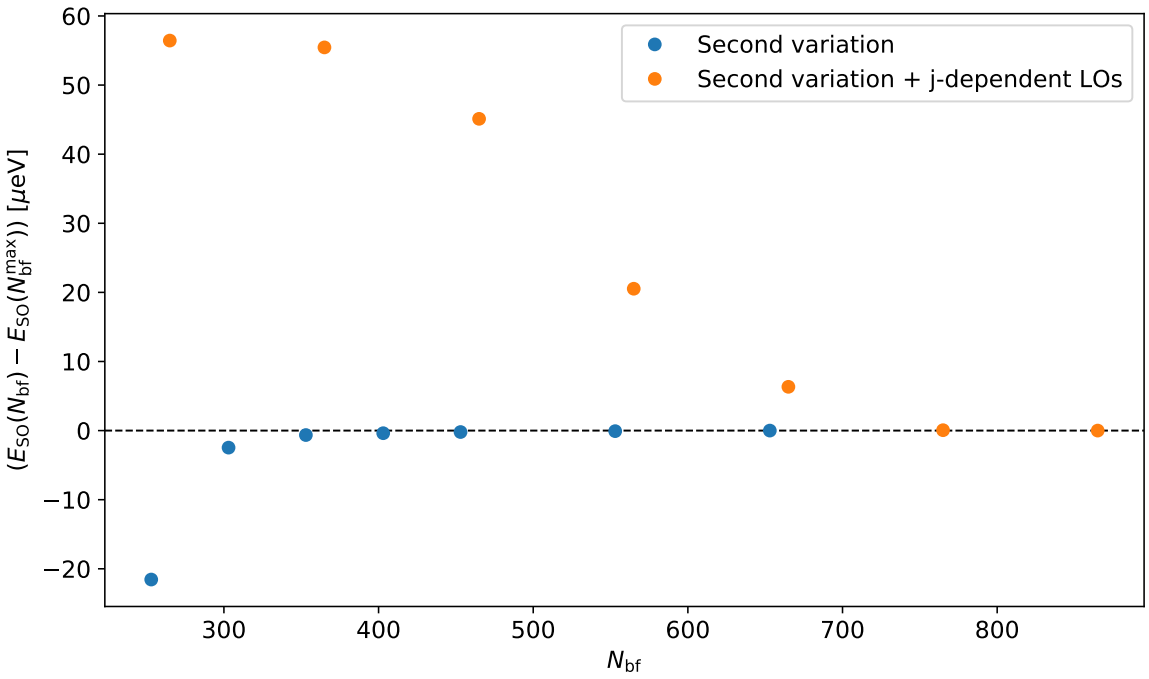

Figure C.2.: Convergence of the computed spin-orbit-splitting of the lowest unoccupied state at K in PbI_2 with respect to the number of basis functions. The zero energy is set to the converged value.

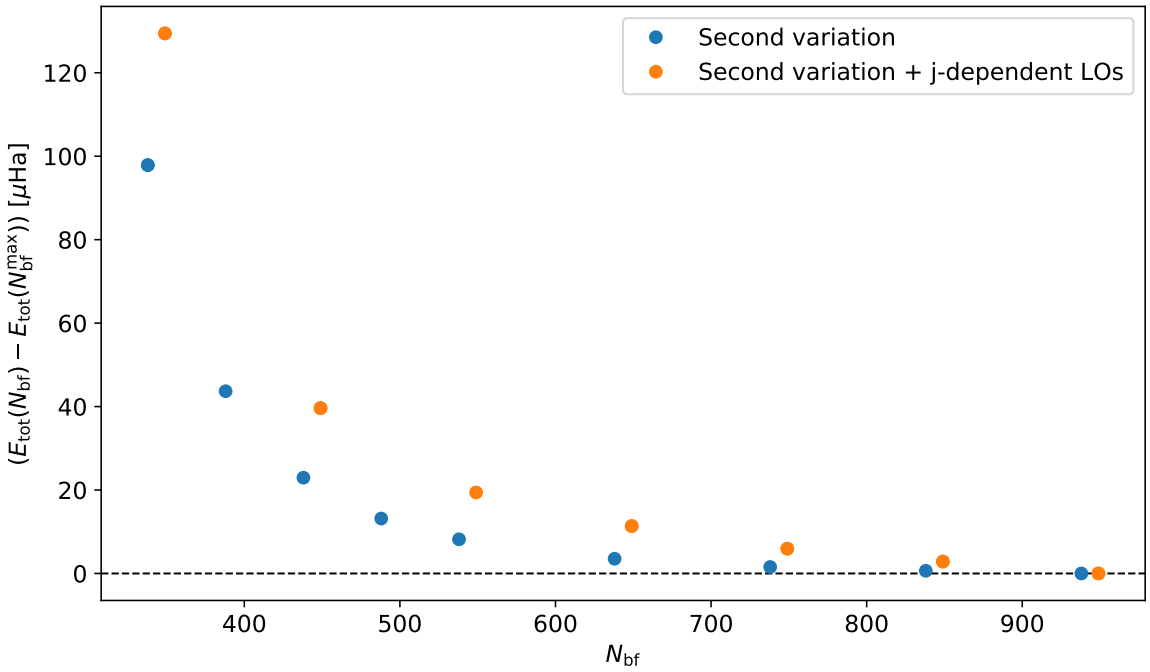

Figure C.3.: Convergence of the computed $CsPbI_3$ total energies with respect to the number of basis functions. The zero energy is set to the converged value.

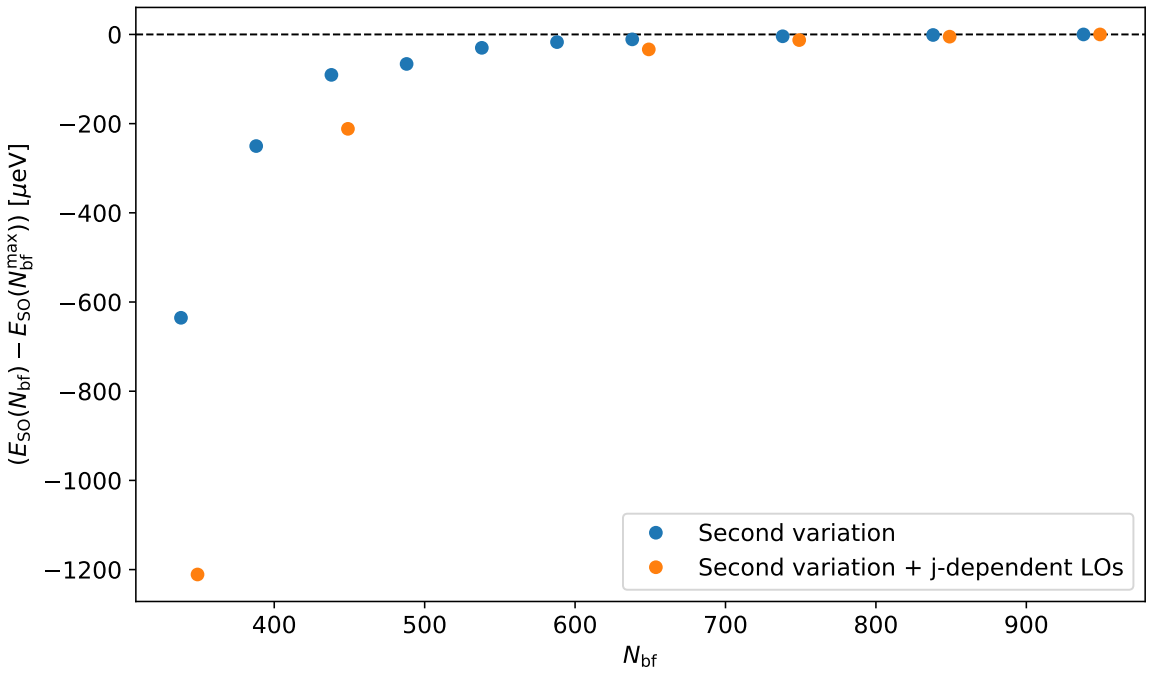

Figure C.4.: Convergence of the computed spin-orbit splitting of the lowest unoccupied state at M in $CsPbI_3$ with respect to the number of basis functions. The zero energy is set to the converged value.

Selbstständigkeitserklärung

Ich erkläre hiermit, dass ich die vorliegende Arbeit selbstständig verfasst und noch nicht für andere Prüfungen eingereicht habe. Sämtliche Quellen einschließlich Internetquellen, die unverändert oder abgewandelt wiedergegeben werden, insbesondere Quellen für Texte, Grafiken, Tabellen und Bilder, sind als solche kenntlich gemacht. Mir ist bekannt, dass bei Verstößen gegen diese Grundsätze ein Verfahren wegen Täuschungsversuchs bzw. Täuschung eingeleitet wird.

Berlin, 17.11.2021, ...